

1 **Multipoint Observations of Compressional Pc5 Pulsations in the Dayside**
2 **Magnetosphere and Corresponding Particle Signatures**
3

4 Galina Korotova^{1,2}, David Sibeck³, Mark Engebretson⁴, Michael Balikhin⁵, Scott
5 Thaller⁶, Craig Kletzing⁷, Harlan Spence⁸, and Robert Redmon⁹
6

7 ¹IPST, University of Maryland, College Park, MD, USA

8 ²IZMIRAN, Russian Academy of Sciences, Moscow, Troitsk, Russia

9 ³NASA/GSFC, Code 674, Greenbelt, MD, USA

10 ⁴Department of Physics, Augsburg University, Minneapolis, MN, USA

11 ⁵Department of Automatic Control and Systems Engineering, University of Sheffield, Sheffield,
12 UK.

13 ⁶LASP, University of Colorado, Boulder, CO, USA

14 ⁷Department of Physics and Astronomy, Iowa University, Iowa City, IA, USA

15 ⁸EOS, University of New Hampshire, Durham, NH, USA

16 ⁹Solar and Terrestrial Physics division, NGDC/NOAA, Boulder, CO, USA

17
18 **Abstract**

19 We use Van Allen Probes Radiation Belt Storm Probes-A and -B (henceforth RBSP-A
20 and -B) and GOES-13 and -15 (henceforth G-13 and G-15) multipoint magnetic field, electric
21 field, plasma, and energetic particle observations to study the spatial, temporal, and spectral
22 characteristics of compressional Pc5 pulsations observed during the recovery phase of a strong
23 geomagnetic storm on January 1, 2016. From ~19:00 UT to 23:02 UT, successive
24 magnetospheric compressions enhanced the peak-to-peak amplitudes of Pc5 waves with 4.5-6.0
25 mHz frequencies from 0-2 to 10-15 nT at both RBSP-A and -B, particularly in the prenoon
26 magnetosphere. Poloidal Pc4 pulsations with frequencies of ~22-29 mHz were present in the
27 radial B_x component. The frequencies of these Pc4 pulsations diminished with increasing radial
28 distance, as expected for resonant Alfvén waves standing along field lines. The GOES
29 spacecraft observed Pc5 pulsations with similar frequencies to those seen by the RBSP, but Pc4
30 pulsations with lower frequencies.

31 Both RBSP-A and -B observed frequency doubling in the compressional component of
32 the magnetic field during the Pc5 waves, indicating a meridional sloshing of the equatorial node
33 over a combined range in Z_{SM} from 0.25 to -0.08 Re, suggesting that the amplitude of this
34 meridional oscillation was ~0.16 Re about an equatorial node whose mean position was near Z_{SM}

35 = ~ 0.08 Re. RBSP-A and -B HOPE and MagEIS observations provide the first evidence for a
36 corresponding frequency doubling in the plasma density and the flux of energetic electron,
37 respectively. Energetic electron fluxes oscillated out of phase with the magnetic field strength
38 with no phase shift at any energy. In the absence of any significant solar wind trigger or phase
39 shift with energy, we interpret the compressional Pc5 pulsations in terms of the mirror mode
40 instability.

41 **Introduction**

42 ULF pulsations with periods of 100 s or greater and high azimuthal wave numbers (m)
43 with magnetic field perturbations in the radial direction and electric field perturbations in the
44 azimuthal direction within the Earth's magnetosphere are typically poloidal waves [Sugiura and
45 Wilson, 1964]. According to Elkington et al. [2003], energetic particles with drift frequencies of
46 6.7-22 mHz and 1.7-6.7 mHz can readily interact with corresponding high-m poloidal Pc4 and
47 Pc5 pulsations. Because the atmosphere and ionosphere screen these high-m waves from the
48 ground, they can only be studied with the help of satellite observations. Past studies of Pc4 and
49 Pc5 pulsations with significant compressional components employed observations from locations
50 at or near geosynchronous orbit [e.g., Dai et al., 2013]. Higbie et al. [1982] and Nagano and
51 Araki [1983] showed that long-lasting compressional Pc5 pulsations occur most frequently in the
52 dayside magnetosphere during the recovery phase of magnetic storms. Storm-time Pc5
53 pulsations occur in the afternoon sector between 12:00 and 18:00 local time following injections
54 of ring current particles [Kokubun, 1985].

55 A number of studies have examined compressional Pc5 waves outside geostationary
56 orbit. According to these studies, compressional Pc5 waves were observed in the dawn
57 [Hedgecock, 1976], dusk [Constantinescu et al., 2009] and noon [Takahashi et al., 1985] sectors.
58 Zhu and Kivelson [1991] reported that intense compressional waves are a persistent feature on
59 both flanks of the magnetosphere. Compressional Pc5 pulsations occur within $\sim 20^\circ$ latitude of
60 the magnetic equator [Vaivads et al., 2001]. They have wavelengths of several radii [Walker et
61 al., 1982] and often exhibit harmonics. Elkington et al. [2003] noted that poloidal and
62 compressional modes are far more effective for the radial transport of energetic particles than the
63 toroidal mode. Two methods are used to identify the harmonic mode of a poloidal oscillation.
64 The first compares the phase difference between the radial component of the magnetic field and
65 the azimuthal component of the electric field [Takahashi et al., 2011]. The second compares
66 observed wave frequencies with the eigenfrequencies predicted by theory [Cummings, 1969].
67 The multi-satellite study of Takahashi et al. [1987a] showed that a compressional Pc 5 wave had
68 an antisymmetric standing structure.

69 Compressional Pc5 pulsations have been ascribed to numerous excitation mechanisms.
70 They can be produced by internal and external processes. It is supposed that the solar wind is the
71 main external source for pulsations produced by the Kelvin-Helmholtz (KH) instability at the
72 magnetopause or the inner edge of the low-latitude boundary layer [e.g., Guo et al., 2010].
73 Observations indicating enhanced rates of Pc5 occurrence during periods of greater solar wind
74 velocity support this model [e.g., Engebretson et al., 1998]. Transient variations in the dynamic
75 pressure of the solar wind or foreshock [e.g., Wang et al., 2018; Shen et al., 2018] that cause
76 abrupt changes in the magnetic field strength in the magnetosphere and sudden impulses in the
77 ionosphere [e.g., Zhang et al., 2010, Sarris et al., 2010] provide another possible trigger for Pc5
78 pulsations. External pressure impulses can cause compressional oscillations of the
79 magnetosphere with discrete eigenfrequencies, known as global modes or cavity/waveguide
80 modes [Samson et al., 1992]. Periodic solar wind dynamic pressure variations directly drive
81 some compressional magnetospheric magnetic field oscillations [e. g., Kepko et al., 2003;
82 Motoba et al., 2003]. Takahashi and Ukhorskiy [2008] considered solar wind pressure variations
83 as the main external driver of Pc5 pulsations observed at geosynchronous orbit in the dayside
84 magnetosphere.

85 Internal generation mechanisms for compressional Pc5 pulsations include the drift-
86 bounce resonant instability which occurs for particles with resonance drift and bounce periods
87 [Southwood et al., 1969] and the drift-mirror instability in the presence of strong temperature
88 anisotropies [Chen and Hasegawa, 1991]. In high β plasmas (β is the plasma pressure divided by
89 the magnetic pressure), these mechanisms favor antisymmetric waves [Cheng and Lin, 1987].

90 One possible generation mechanism for compressional Pc5 pulsations at geosynchronous
91 orbit is a drift-mirror instability of ring current particles [e.g., Lanzerotti et al., 1969]. While
92 the observed anticorrelated magnetic field strength and ion flux oscillations are expected for a
93 drift mirror wave [Kremser et al., 1981], the instability criterion is generally not satisfied
94 [Pokhotelov et al., 1986]. One possible reason for the lack of consistency between theory and
95 observation might be because the real geometry of the magnetosphere is not taken into account
96 [Cheng and Lin, 1987]. Compressional pulsations are often accompanied by pulsations in
97 particle fluxes [Kremser et al., 1981; Liu et al., 2016]. Particle observations can provide useful
98 information on the spatial and wave structure of ULF pulsations. Lin et al. [1976] explained
99 flux oscillations as the adiabatic motion of particles in a magnetohydrodynamic wave.
100 Kivelson and Southwood [1985] studied charged particle behavior in compressional ULF
101 waves and showed that “a mirror effect” is the dominant cause for particle flux modulations.
102 Finite gyroradius effects enable detection of gradients in particle flux associated with waves
103 [e.g., Korotova et al., 2013].

104 We use multipoint magnetic field, plasma, and energetic particle observations from RBSP-A
105 and -B and G-13 and -15 to study the spatial, temporal, and spectral characteristics of
106 compressional Pc5 pulsations observed deep within the magnetosphere during the recovery
107 phase of the strong magnetic storm which began on December 31, 2015. We investigate the type
108 of pulsation (compressional versus transverse), their harmonic mode, and their latitudinal nodal
109 structure. We focus on the properties of double frequency pulsations that occurred in the vicinity
110 of the geomagnetic equator. We demonstrate that the energetic particles respond directly to the
111 compressional Pc5 pulsations and also exhibit a double frequency oscillation. We search for
112 possible solar wind triggers and test two possible generation mechanisms: drift-bounce
113 resonance, and mirror instability. The paper is organized as follows: Section 2 describes
114 instruments and resources. Section 3 presents the solar wind and IMF conditions. Section 4
115 provides an analysis of these waves and their generation mechanisms.

116 **2. Resources**

117 The Van Allen Probes mission can be used to study the geospace response to a
118 fluctuating solar wind. The mission began in August 2012 with a twin spacecraft launch into
119 similar 10° inclination orbits with perigee altitudes slightly greater than 600 km and apogee
120 altitudes just beyond 30000 km [Mauk et al., 2012]. The spacecraft carry instruments that
121 measure electromagnetic fields, waves, and charged particle populations deep within the
122 magnetosphere. This paper employs observations of the most abundant ion components as well
123 as electrons, over the 0.001–50 keV energy range of the core plasma populations from the
124 HOPE instrument, populations of 20–4000 keV ion and electrons from the MagEIS instrument
125 [Blake et al., 2013] in the Energetic Particle, Composition, and Thermal (ECT) suite [Spence et
126 al., 2013], fluxes of ions over the energy range from ~20 keV to ~1 MeV and electrons over
127 the energy range ~25 keV to ~1 MeV (RBSPICE) [Mitchell et al., 2013] in conjunction with
128 observations from the magnetometer in the Electric and Magnetic Field Instrument Suite and
129 Integrated Science suite (EMFISIS) [Kletzing et al., 2013], and the Electric Field and Waves
130 (EFW) [Wygant et al., 2013] instrument. We examine electric and magnetic field measurements
131 with 11 s and 4 s time resolution, respectively, and differential particle flux observations with
132 ~11 s (spin period) time resolution. The data are provided by NASA/GSFC's CDAWEB in the
133 MGSE (modified GSE) coordinate system. We use magnetic field data from G-13 and -15 with
134 0.5 s time resolution [Singer et al., 1996]. Finally, we employ Wind solar wind magnetic field
135 and 3DP plasma data with 3 s time resolution [Lepping et al., 1995; Lin et al., 1995].

136

137 **3. Orbit and solar wind and geomagnetic conditions**

138 Figure 1 presents the Bz component of the interplanetary magnetic field observed at
139 Wind, and geomagnetic activity Dst and AE indices obtained from the OMNI database (upper
140 panels) from 12:00 UT on December 30 to 00:00 UT on January 2, 2016. The bottom panels
141 show Wind observations of the magnetic field components, total magnetic field strength, cone
142 angle, pressure, plasma density, and velocity from 16:00 UT on January 1, 2016 to 00:00 UT on
143 January 2, 2016 during which time the spacecraft moved from GSM (X, Y, Z) = (194.7, 20.1, -
144 12.5) Re to (194.8, 23.6, -7.4) Re. The pulsation events to be studied here occurred late on
145 January 1, 2016, following a prolonged period of strongly southward IMF orientation and
146 geomagnetic activity. A substantial increase in the solar wind dynamic pressure early on
147 December 31 was followed by a strong southward IMF that persisted from 19:00 UT on
148 December 31, 2015 until 09:00 UT on January 1, 2016. A strong electrojet with AE index
149 greater than 2100 nT at 12:36 UT on December 31, 2015 was followed by two moderate
150 substorms that enhanced AE at ~14:00 and 18:45 UT on January 1, 2016. The Dst index
151 responded by reaching a value as low as -110 nT at 00:30 UT on January 1, 2016. Shading
152 highlights the interval from ~19:00 to 23:02 UT late in the recovery phase and late in the day on
153 January 1, 2016 when the Van Allen Probes and GOES spacecraft observed the strong
154 compressional Pc5 pulsations of interest to this study.

155 The latter interval (bottom panels) was marked by strong variations in the solar wind
156 dynamic pressure. Shading marks an interval of depressed magnetic field strengths and
157 generally anticorrelated enhanced densities, velocities and solar wind dynamic pressures. The
158 cone angle, θ , defined as the angle between the IMF and the Sun-Earth line was less than 45^0
159 during this interval. The magnetic field was briefly aligned with the Sun-Earth line (Bx) at the
160 center of the interval from 20:00-21:00 UT. For most of the ~4h long shaded interval, IMF Bx
161 (By) was predominantly positive (negative) and the Bz component remained almost constant
162 near 0 nT, indicating a spiral and equatorial IMF configuration. The total magnetic field strength
163 decreased from 7.9 nT at 18:00 UT to 2.2 nT at 19:48 UT and the solar wind velocity and
164 dynamic pressure increased from 426 km/s and 0.62 nPa at 18:00 UT to 457 km/s and to 3.37
165 nPa at 20:47 UT, respectively. At ~ 22:20 UT almost all parameters returned to their initial
166 undisturbed values.

167 Figure 2 presents RBSP-A and -B and G-13 (MLT~ UT-5) and -15 (MLT~ UT- 9)
168 trajectories from 15:00 UT to 24:00 UT on January 1, 2016 in the X-Y and X-Z GSM planes.
169 Open circles mark the beginning of the spacecraft trajectories which are duskward for the GOES
170 spacecraft and duskward at apogee for the Van Allen Probes. All of the spacecraft were north of
171 the equator when in the dayside magnetosphere. The thick line segments (dots) indicate the
172 locations of the spacecraft at the times when (weak) Pc5 magnetic field pulsations occurred.

173 Figure 3 compares lagged Wind solar wind dynamic pressure variations with G-13 and -
174 15 observations of the dayside magnetospheric magnetic field. The arrows connect
175 enhancements of the solar wind dynamic pressure to corresponding compressions of the
176 magnetosphere. To determine the lag time between the Wind and GOES-15 observations we
177 related individual magnetosphere compressions to corresponding dynamic pressure variations.
178 Additionally, we confirmed these empirically derived lag times with simple ballistic estimates
179 based on the solar wind velocity and the distance of Wind from Earth. It is relatively easy to
180 associate the GOES magnetic field enhancements with corresponding features in the solar wind
181 dynamic pressure at the beginning and the end of the interval but less easy from 19:50 UT to
182 21:20 UT corresponding to ~ 20:45 UT and 22:15 UT at the GOES spacecraft. The lag time
183 from Wind to the Earth is not uniform and depends on IMF orientation. At the beginning and
184 end of the interval, when the IMF was spiral ($B_x > 0$, $B_y < 0$), the lag was in the range of ~46 to
185 58 min. Consistent with expectations, the lag became greater for the interval from ~ 19:50 UT to
186 21:20 when the IMF was nearly radial (B_y and $B_z \sim 0$ nT). The reasonable correspondence of the
187 magnetosphere compressions to solar wind dynamic pressure variations demonstrates that Wind
188 was a good monitor for solar wind conditions and that a series of pressure enhancements were
189 applied to the magnetosphere during the interval of interest. Pc5 pulsation amplitudes at G-13
190 and -15 were greater during the interval of enhanced solar wind dynamic pressure and
191 magnetospheric magnetic field strengths than they were at earlier and later times.

193 **4. Pulsation Observations**

194 **4.1. Spatial characteristics of Pc5 pulsations**

195 Consider the spatial extent, temporal, and spectral characteristics of the compressional
196 Pc5 pulsations. Figure 4a shows G-13 and -15 observations of the total magnetic field strength
197 from 18:00 UT to 24:00 UT. The spacecraft observed long-duration Pc5 pulsations over a wide
198 longitudinal region in the pre- and post-noon magnetosphere from 10:00 to 15:20 MLT (Figure
199 2). G-15 observed weak, less than ~5 nT amplitude, Pc5 waves from 18:28 UT to 19:04 UT
200 prior to the main event. During the main event from 19:04 to 23:00 UT, the magnetosphere was
201 compressed (Figure 3), magnetic field strengths increased and the amplitude of these waves
202 increased to values ranging from 10 to 16 nT with peak amplitudes prior to local noon. G-13
203 observed weak Pc5 pulsations with amplitudes of 2-4 nT throughout most of the time interval
204 from 16:40 UT (not shown) to 21:00 UT. During the interval from 19:34 UT (~14:45 MLT) to
205 20:10 UT (~15:20 MLT), the pulsations reached slightly stronger amplitudes of 5-8 nT. At
206 23:02 UT all Pc5 wave activity at both GOES stopped.

207 Figure 4b shows the RBSP-A and -B total magnetic field strength from 18:40 UT to 21:10
208 UT and from 20:40 UT to 23:10 UT, respectively, on January 1, 2016. Taken together, RBSP-A
209 and -B observed Pc5 pulsations that occupied the inner dayside magnetosphere from 5.26 to 5.75
210 RE and from 09:56 to 12:44 MLT (Figure 2). Prior to the arrival of the strong solar wind
211 dynamic pressure variations from 18:15 to 18:55 UT RBSP-A observed very weak pulsations
212 with Pc5 periods and amplitudes of 1-3 nT (not visible at this scale). After the compression of
213 the magnetosphere just after 19:00 UT, the pulsation amplitude at RBSP-A increased to values
214 ranging from 10 to 15 nT with the peak amplitude occurring prior to local noon (Figure 4b).
215 RBSP-B observed similar compressional Pc5 pulsations from 20:46 UT that ceased
216 simultaneously with the end of the magnetospheric compression at about 23:02 UT.

217 To determine the type of the Pc5 waves we converted the magnetic field observations
218 from GSE into field-aligned coordinates (FAC). Here the Z axis lies parallel to the locally-
219 averaged magnetic field. The Y axis points approximately azimuthally eastward and is transverse
220 to B and to the outward radius vector. The X axis completes the right-handed system and is
221 directed approximately radially outward from Earth. Figure 5 presents RBSP-A and -B magnetic
222 field observations in FAC. The Bz component is the value of the total magnetic field after
223 subtraction of a 16-minute sliding average. The Pc5 pulsations are observed in all three
224 components but the amplitudes of the azimuthal By and radial Bx components are rather small
225 and do not exceed 7 nT. The compressional Bz component is much more pronounced for both
226 spacecraft, reaching amplitudes of 14-15 nT before local noon. Consequently, the pulsations are
227 primarily compressional. The Bz component oscillated out of phase with the Bx component at
228 RBSP-A and in phase at RBSP-B and in quadrature with the By component. Simultaneous
229 RBSP-A and -B electric and magnetic field measurements provide an opportunity to study the
230 mode of the Pc5 waves. Determining the harmonic mode of the Pc5 waves requires us to
231 consider the phase of the azimuthal component of the electric field Ey with respect to the radial
232 component of the magnetic field Bx as a function of latitude [Takahashi et al., 2011]. Figure 6
233 shows that the phase of the Ey component leads that of the Bx component by 90° at RBSP-A
234 from 19:10 UT to 20:00 UT and therefore the Pc5 waves are second harmonic in nature.

235

236 **4.2. Spectral characteristics**

237 We calculated dynamic spectra for the magnetic field pulsations. Figure 7 presents the
238 radial, azimuthal and compressional components of the dynamic spectra of the magnetic field at
239 RBSP-A and -B from 18:00 to 21:10 UT and from 20:00 UT to 23:10 UT on January 1, 2016,
240 respectively. The color bar on the right shows the scale for power for frequencies ranging from
241 0 to 41 mHz in each component. The magnetic field exhibited several wide-band enhancements

at frequencies ranging from 4 to 29 mHz. As expected for compressional Pc5 pulsations, both GOES spacecraft observed the strongest power densities in the Bz component at dominant frequencies of \sim 4.5-6 mHz. Red arrows in the Bz panels of Figure 7 for RBSP-A and -B indicate the double frequency pulsations at \sim 5.5 mHz and \sim 11 mHz. We calculated Fourier spectra for the three components of the RBSP-A and -B magnetic field in 600 second sliding-averaged mean FAC for each thirty minute interval during the event. Figure 8 presents examples of Fourier spectra calculated for the RBSP-A and -B magnetic field from 19:30 UT to 20:00 UT and from 22:30 UT to 23:00 UT, respectively, on January 1, 2016. The red arrows show the dominant frequencies at 5.5 and 5 mHz observed at the two spacecraft, corresponding to periods of 170-200 s. RBSP-A and -B were situated three hours in local time apart; the similar frequencies indicate that conditions in the dayside magnetosphere remained steady for a long time and over a broad region.

In passing, we note the presence of Pc4 pulsations. Returning to Figure 7, we see enhanced power densities at frequencies of \sim 22-29 mHz with dominant frequencies from 23 to 27 mHz primarily in the radial Bx component. These can be ascribed to poloidal Pc4 produced simultaneously with the Pc5 but likely with another energy source. The frequencies of the Pc4 pulsations decrease with increasing radial distance, as expected for resonant standing Alfvén waves [Sugiura and Wilson, 1964]. Pulsation periods depend upon the magnetic field line length, the magnetic field magnitude, and the ion density. Shorter field line lengths and enhanced magnetic field strengths closer to Earth decrease pulsation periods. Blue arrows in Figure 8 indicate Pc4 pulsations at \sim 25-27 mHz.

Figure 9 presents dynamic spectra for the G-13 and -15 magnetic field in FAC from 18:00 UT to 24:00 UT on January 1, 2016. Spectral power was calculated for frequencies from 0 to 48 mHz. Like the RBSP-A and -B magnetic field spectra, there are two broad frequency band enhancements corresponding to Pc4 and 5 frequencies. The dominant frequencies for the compressional Pc5 pulsations occur from 4.5 to 6.5 mHz. These frequencies are similar to those observed by Van Allen Probes and we suppose that they were generated by the same sources. The Pc4 pulsations are most pronounced in the radial Bx component and display strongest spectral power densities in the frequency range from 13 to 21 mHz. These frequencies are lower than those observed by Van Allen Probes, since the GOES spacecraft were located further radially outward from Earth [Sugiura and Wilson, 1964]. The frequencies of the long-lasting Pc4 pulsations observed by G-15 depended on local time. They decreased from 20-22 mHz in the prenoon magnetosphere to 14-17 mHz near local noon, perhaps in response to differing conditions (e.g., densities). Takahashi et al. [1984] noted that an increase in plasma mass density from morning to afternoon is typical at geosynchronous orbit. Since the frequencies of the Pc4

277 pulsations depended on local time and radial distance from Earth, their sources must be more
278 localized than those for the Pc5 pulsations.

279

280 **4.3. Particle signatures**

281 Energetic particle observations provide further information concerning this event. We
282 inspected RBSP-A and-B MagEIS observations of energetic particles from 18:30 UT to 21:00
283 UT and from 20:40 UT to 23:10 UT on January 1, 2016, respectively, and found that the
284 intensities of electrons with energies from tens of keV to 2 MeV oscillated with Pc5 periods
285 corresponding to those of the magnetic field. Figures 10a and b show an example of RBSP-A
286 observations of electron fluxes (a) in the energy range of from 31.5 keV to 1704 keV from
287 18:30 UT to 21:00 UT and (b) their expanded view for selected energies from 19:20 UT to
288 20:00 UT. The energetic electron fluxes oscillated out of phase with the compressional Bz
289 component of Pc5 magnetic field pulsations and did not display any phase differences across all
290 energies. The depth of modulation (the peak to valley ratio) is larger for higher energy electrons
291 consistent with the results of Liu et al. [2016] who interpreted similar observations in terms of
292 mirror mode waves. The lower energy electron fluxes displayed more noticeable enhancements
293 as a response to the compressions of the magnetosphere. Kivelson and Southwood [1985] noted
294 that the maintenance of pressure balance in low- frequency compressional waves usually
295 requires the presence of some pitch angle anisotropy and the antiphase relation between the
296 plasma and magnetic field pressures suggests that particle pitch angle distributions peak near
297 90°. Figure 11 presents RBSP-A and -B observations of pitch angle distributions for electrons
298 with energies from 54 keV to 1060 keV from 18:30 to 21:00 UT and from 20:40 UT to 23:10 UT
299 on January 1, 2016, respectively. The figure confirms that pitch angle distributions peak near
300 90°. Furthermore, it shows that the electron intensities display quasi-periodic enhancements at
301 all energies with the strongest at pitch angles near 90°.

302

303 **4.4. Double-frequency pulsations**

304 When RBSP-A and -B were in the vicinity of the geomagnetic equator the compressional
305 Pc5 pulsations displayed peculiar features indicating frequency doubling. The compressional
306 components oscillated with a frequency twice that of the transverse component. Coleman [1970]
307 was the first to report observations of such events in the geosynchronous magnetic field.
308 Higuchi et al. [1986] called them harmonic structures when the first and second harmonics
309 exhibited similar amplitudes and transitional structures when the amplitudes of the alternating
310 peak were different. Takahashi [1987b] interpreted double-frequency oscillations in terms of a
311 model invoking the second harmonic structure of an antisymmetric standing wave in which the

location of the equatorial node of field-lined displacement oscillates in phase with the wave. Cheng and Qian [1994] presented a model for the magnetic field perturbations during the pulsations reported by Takahashi et al. [1987a, 1990]. Figure 6 in the paper of Korotova et al. [2013] illustrates how low-latitude spacecraft can observe two magnetic field strength enhancements per wave cycle when the equatorial node oscillates latitudinally up and down in phase with an antisymmetric compressional wave. Right at the equator the spacecraft observes identical amplitudes for the two compressions. At any other latitude the two compressions at the spacecraft will have different magnitudes and the imbalance between them increases when the spacecraft moves farther from the equator. Takahashi et al. [1997b] showed that that a latitudinal shift of a fraction of degree can turn a harmonic B_z structure into a nonharmonic structure. Spacecraft located far from the magnetic equator do not observe frequency doubling, just a single enhancement. Korotova et al. [2013] derived the latitudinal structure of the waves by invoking north-south sloshings of the low-latitude node.

Figures 12a and b present (a) RBSP-A and -B observations of double frequency magnetic pulsations and (b) their locations in the X-Y GSM and X-Z SM planes. Dashed lines in Figure 12a indicate intervals when the double frequency pulsations in B_z are most prominent: 20:45-20:54 UT at RBSP-A and 21:03 UT to 21:31 UT at RBSP-B in these line plots. However, the amplitudes of the second harmonic are generally much lower than those of the first harmonic. At these times, e.g. from 20:05 to 20:45 UT at RBSP-A and 21:35-21:55 UT at RBSP-B, the second harmonic compressions in B_z are barely perceptible in these line plots. Model predictions for the magnetic field perturbations associated with an equatorial node whose latitude oscillates in phase with an antisymmetric poloidal wave indicate that the ratio of the amplitudes of the first to second harmonic compressions should change with latitude, being ~ 1 at the average position of the low-latitude node and ~ 0 at and beyond the maximum latitude to which the oscillating node can reach [Takahashi et al., 1987b]. To determine the meridional motion of the magnetic field node we measured amplitudes of the first and second harmonics of the compressional pulsations. We found that RBSP-A observed ratios near 1 at $Z_{SM} = \sim 0.08$ Re while RBSP-B observed ratios near 1 at $Z_{SM} = \sim 0.10$ Re. These are the locations where the southward-moving spacecraft pass through the mean positions of the equatorial node. Figure 12a shows that RBSP-A observed second harmonics from $Z_{SM} = 0.25$ to 0.04 Re, while RBSP-B observed them from $Z_{SM} = 0.19$ to -0.08 Re. Consequently, we believe that the equatorial node oscillated with an amplitude of at least 0.15 to 0.18 Re. Note however, that the ratio of the first to second harmonics does not show a smooth transition as the spacecraft move equatorward. Either the amplitude of the compressional pulsation or the meridional oscillation in the equatorial node varied in time, probably abruptly.

347 Figures 10a and b show that the compressional pulsations modulated energetic electrons
348 observed by RBSP-A and we should therefore expect to find the signatures of the double-
349 frequency pulsations not only in the magnetic field but also in the fluxes of particles. Takahashi
350 et al. [1990] reported AMPTE/CCE observations of compressional Pc5 pulsations that exhibited
351 harmonically related transverse and compressional magnetic oscillations that modulated the flux
352 of medium energy protons ($E > 10$ keV) with double frequency but did not discuss the event in
353 detail. We report the first evidence for meridional sloshing of the equatorial node in the
354 simultaneous compressional Pc5 pulsations and variations of electrons fluxes and electron
355 densities observed by MagEIS and Hope, respectively. Figure 13 presents RBSP-A (left panel)
356 and -B (right panel) electron fluxes for energies at 31.9 keV and 54.8 keV, electron densities and
357 the B_z component of the magnetic field in FAC from 19:00 UT to 21:00 UT and at RBSP-B
358 from 20:46 UT to 22:10 UT. The panels in the bottom of Figure 13 present expanded views of
359 20 min intervals with the double-frequency pulsations. The B_z component of the magnetic field
360 varies with double frequencies out of phase with the fluxes of electrons and densities. This study
361 gives better insight into the nodal structure of the waves and helps to clarify their source.

362

363 **4.5. Testing Pc4-5 pulsation generation mechanisms**

364 We tested several causes for the Pc4-5 pulsations, including solar wind pressure pulses,
365 the KH instability on the magnetopause, drift-bounce resonant particle interactions, and the
366 mirror-mode instability. First, with the exception of the interval from 19:35 UT to 19:55 UT, the
367 Wind observations shown in Figure 1 provide no evidence for periodic solar wind drivers in the
368 Pc5 range, be they density variations or IMF fluctuations; thus ruling out solar wind pressure
369 pulses as the direct cause of the Pc4-5 pulsations. We then considered the possibility of KH
370 waves. These waves are expected when the solar wind velocity is high and both the
371 magnetosheath and magnetospheric magnetic fields lie transverse to the magnetosheath flow, i.e.
372 on the flanks of the magnetosphere when the IMF points southward or in particular northward
373 [e.g., Guo et al., 2010]. As shown in Figure 1, the solar wind velocity during the interval when
374 the Pc5 events occurred was only moderate, 400-460 km/s. Furthermore, the IMF did not point
375 either strongly northward or southward. Therefore, we conclude that the compressional Pc5
376 pulsations were excited by processes internal to the magnetosphere.

377 Southwood [1981] and Kivelson and Southwood [1985] described how the resonant drift-
378 bounce interaction of particles with an azimuthally-propagating wave generates large amplitude
379 ULF waves in an inhomogeneous background field. For this to happen, the wave frequency ω
380 must satisfy the resonance condition:

381
$$\omega - m\omega_d - N\omega_b = 0, \quad (1)$$

382 where ω_d and ω_b are the angular drift and bounce frequencies, N is an integer, and m is the
383 azimuthal wave number. Southwood [1973] predicted that particle flux oscillations just above
384 and below the resonant energy should be 180° out of phase. As Figures 10a and b demonstrate,
385 RBSP-A did not observe any such phase reversal in the electrons as a function of energy. We
386 exclude the drift-bounce resonance as the cause of these compressional Pc5 pulsations.

387 Finally, we examined the mirror instability criterion. The mirror instability is a kinetic
388 phenomenon that occurs spontaneously in anisotropic high β plasmas when the ratio of
389 perpendicular to parallel pressures is large [Southwood and Kivelson, 1993]. The test for the
390 mirror instability is approximately:

391
$$\Gamma = 1 + \beta_{\perp} [1 - T_{\perp}/T_{\parallel}] < 0, \quad (2)$$

392 where $T_{\parallel, \perp}$ are the plasma temperatures parallel and perpendicular to the ambient magnetic field
393 and β_{\perp} is the ratio of the perpendicular component of the thermal plasma pressure to the
394 magnetic pressure. For our calculations we obtained the magnetic field data from EMFISIS and
395 thermal plasma pressures perpendicular and parallel to the magnetic field from RBSPICE. We
396 used the density and temperature from HOPE to calculate the parallel and perpendicular thermal
397 pressures within the energy range covered by this instrument, but found these pressures to be
398 small compared to those from RBSPICE. Consequently, our calculations neglect the
399 contributions from HOPE to the thermal pressures.

400 Figures 14a and b show RBSP-A and -B plasma and magnetic field parameters
401 characterizing the pulsations. The upper panels indicate that magnetic field and plasma pressures
402 vary in antiphase during the Pc5 pulsations. However, the total pressure is not balanced as might
403 be expected for mirror mode waves. We suppose that this is because the RBSPICE (or even the
404 RBSPICE + HOPE) plasma instruments do not observe the entire plasma distribution. Assuming
405 that the total plasma pressure is proportional to the fraction that RBSPICE does observe, we
406 scaled the thermal plasma pressures observed by RBSPICE upward to values that cause the sum
407 of the magnetic and perpendicular thermal plasma pressure variations associated with the waves
408 to be approximately constant during the intervals from 19:03 UT to 19:14 UT for RBSP-A and
409 from 22:32 UT to 22:56 UT for RBSP-B. The upward scaling factors were 1.97 and 1.69,
410 respectively. We then applied these factors to both the perpendicular and parallel pressures. The
411 third panels of Figures 14a and b show the values of β_{\perp} calculated from these scaled pressures.
412 Shaded grey areas in the fourth panels show when the drift mirror instability is satisfied (< 0).
413 As the test for the mirror instability is satisfied throughout most of the intervals of enhanced
414 temperature (pressure) anisotropy and $\beta > 1$ at RBSP-A and -B, we attribute the compressional
415 Pc5 pulsations observed on January 1, 2016 to the mirror instability.

416

417 **Conclusions**

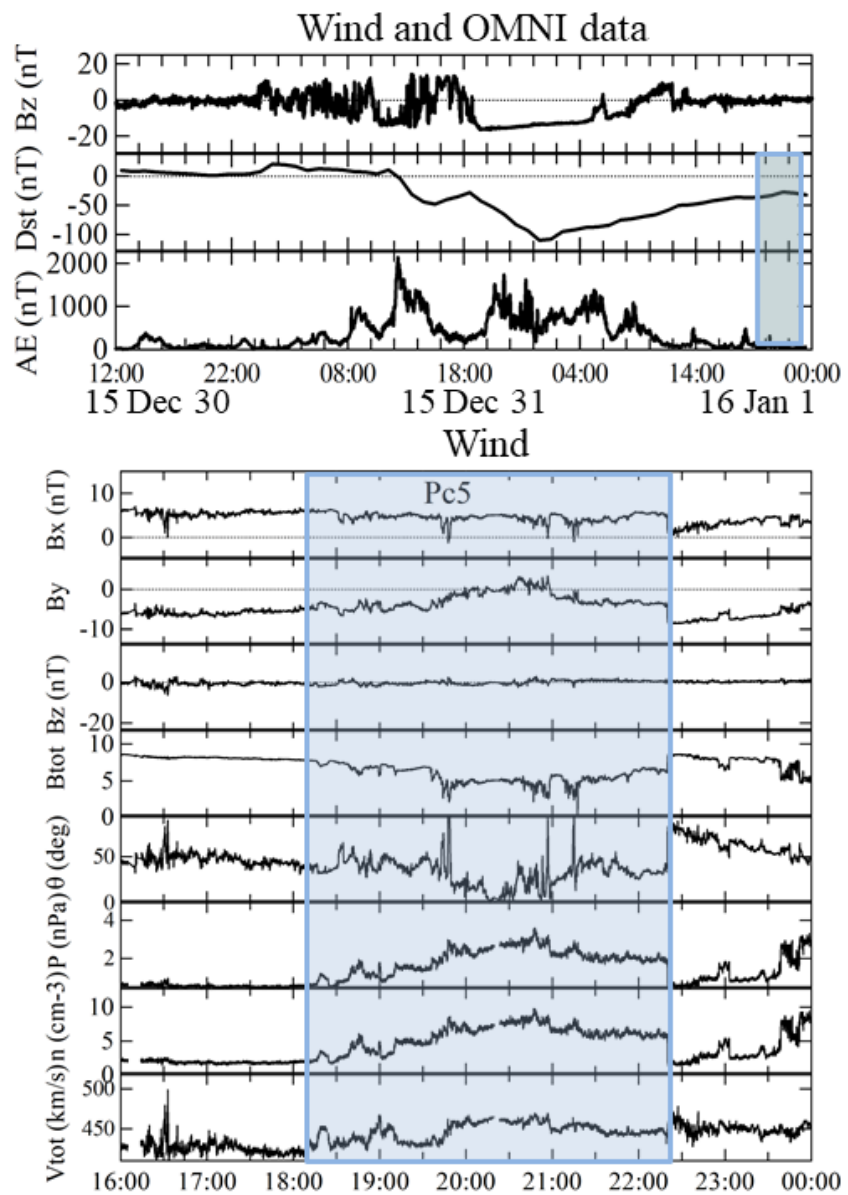
418 We used Van Allen Probes and GOES multipoint magnetic field, electric field, plasma
419 and energetic particle observations to study the nature of compressional Pc5 pulsations at the end
420 of a strong magnetic storm on January 1, 2016. From \sim 19:00 UT to 23:02 UT the
421 magnetosphere was compressed and transient increases of the total magnetic field strength
422 occurred every 20-40 min. During this interval the spacecraft observed compressional Pc 5
423 pulsations over a large longitudinal extent. The solar wind pressure enhancements initiated
424 and/or amplified compressional wave activity in the dayside magnetosphere. The pulsations
425 occupied the dayside magnetosphere from 5.26 to 6.6 Re and from 09:56 to 15:20 MLT.
426 Successive solar wind pressure increases and magnetospheric compressions enhanced the
427 amplitude of Pc5 wave activity to values from 10 to 16 nT. The strongest amplitudes occurred
428 prior to local noon. They were observed when the IMF cone angle was less than 45°. We
429 studied the wave mode of the Pc5 pulsations and found that they had an antisymmetric
430 structure.

431 The greatest spectral power densities observed at RBSP-A and -B occurred in the
432 north/south, or B_z , component of the magnetic field at frequencies of \sim 4.5-6.0 mHz. The two
433 spacecraft observed similar frequencies, indicating that conditions within the dayside
434 magnetosphere remained steady for a long time and over a broad region. Enhanced spectral
435 power densities at frequencies of \sim 22-29 mHz in the radial B_x component can be attributed to
436 the simultaneous generation of poloidal Pc4 pulsations by a different mechanism. The
437 frequencies of the Pc4 pulsations diminished with increasing radial distance. The dominant
438 frequencies for the compressional Pc5 pulsations observed by GOES resembled those observed
439 by RBSP-A and -B and we suppose that they were generated by the same sources. Pc4 pulsations
440 observed by the GOES spacecraft displayed frequencies that were
441 lower than those observed by RBSP-A and -B, since the GOES spacecraft were located further
442 radially outward from Earth. Since the frequencies of the Pc4 pulsations depended on local time
443 and radial distance from Earth, their sources must be more localized than those for the Pc5
444 pulsations.

445 When the spacecraft were in the vicinity of the geomagnetic equator, RBSP-A observed
446 meridional sloshing of the equatorial wave node from $Z_{SM} = 0.25$ to 0.04 Re, while RBSP-B
447 observed them from $Z_{SM} = 0.19$ to -0.08 Re. Consequently, we believe that the motion of the
448 meridional oscillation of the position of the equatorial node was at least 0.15 to 0.18 Re. We
449 found that RBSP-A observed ratios near 1 at $Z_{SM} = \sim$ 0.08 Re while RBSP-B observed ratios near
450 1 at $Z_{SM} = \sim$ 0.10 Re. These were the locations where the southward-moving spacecraft RBSP-A
451 and -B passed through the mean positions of the equatorial node at $Z_{SM} = \sim$ 0.08 Re and at $Z_{SM} =$

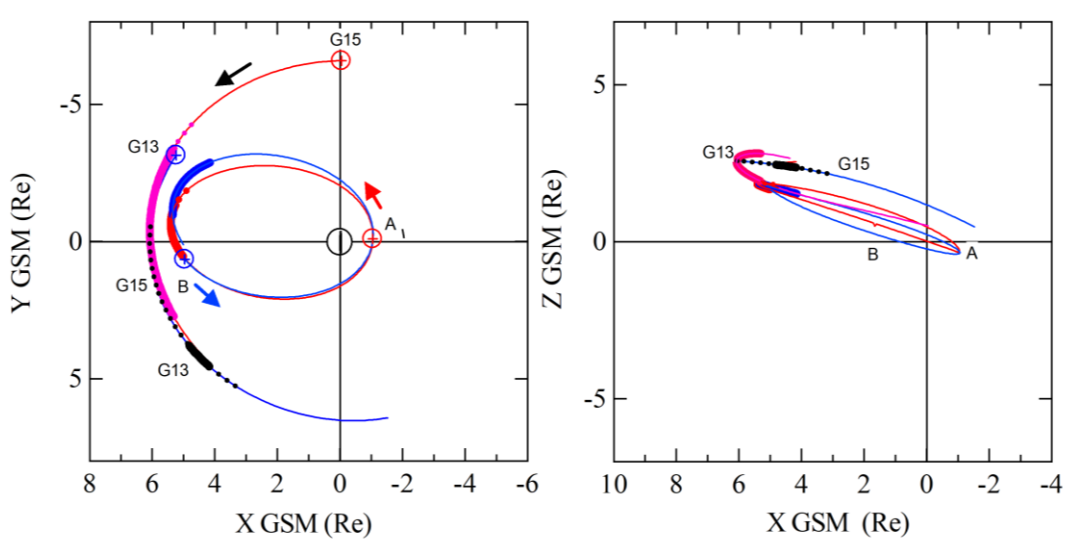
452 ~0.10 Re, respectively. We report the first evidence for meridional sloshing of the equatorial
 453 node in the double-frequency variations of electrons fluxes and electron density observed by
 454 MagEIS and HOPE, respectively.

455 The energetic particles observed by RBSP-A and -B showed a regular periodicity over a
 456 broad range of energies from tens of eV to 2 MeV with periods corresponding to those of the
 457 compressional component of the ULF magnetic field. The electron intensities exhibited quasi-
 458 periodic enhancements at all energies with the most intense at pitch angles near 90°. The
 459 energetic electron fluxes oscillated out of phase with the magnetic field and did not display any
 460 phase shift across all energies. The depth of modulation was larger for higher energy electrons.
 461 We searched for possible solar wind triggers and discussed generation mechanisms for the
 462 compressional Pc5 pulsations in terms of drift mirror instability and drift bounce resonance. We
 463 interpret the compressional Pc5 waves in terms of drift-mirror instability.

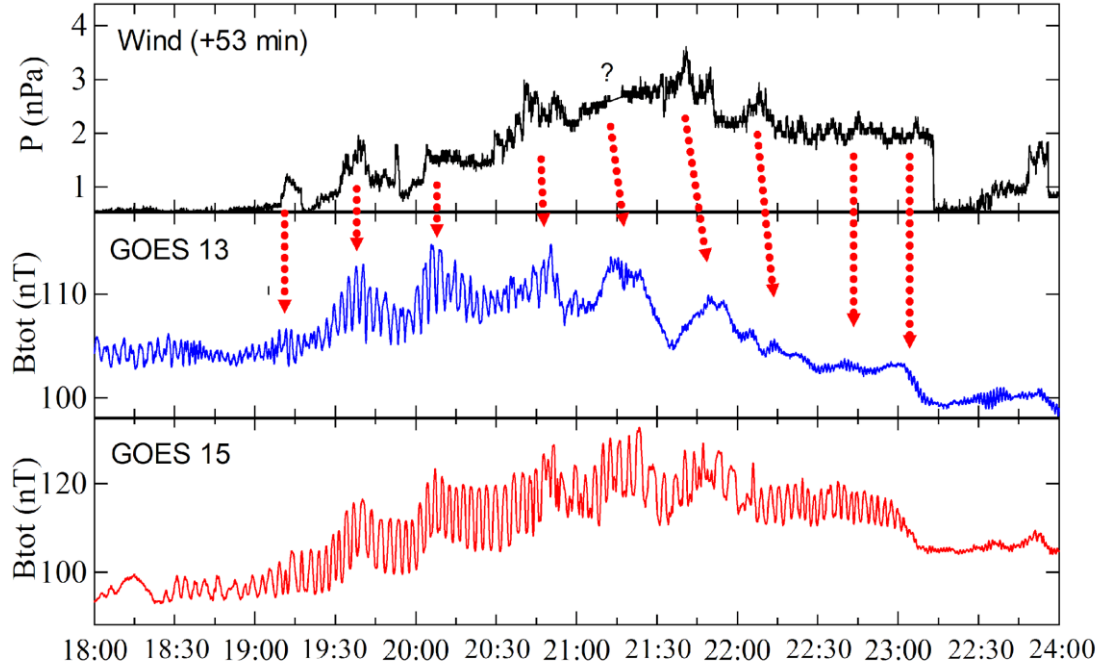


464

465 Figure 1. Bz component of the magnetic field observed at Wind, and geomagnetic activity Dst
 466 and AE indices obtained from the OMNI database (upper panels) from 12:00 UT on December
 467 30 to 00:00 UT January 2, 2016. The bottom panels show Wind observations of the magnetic
 468 field components, total magnetic field strength, cone angle, pressure, plasma density, and
 469 velocity from 16:00 UT on January 1, 2016 to 00:00 UT on January 2, 2016. Shading highlights
 470 intervals when magnetospheric spacecraft observed Pc5 compressional pulsations.

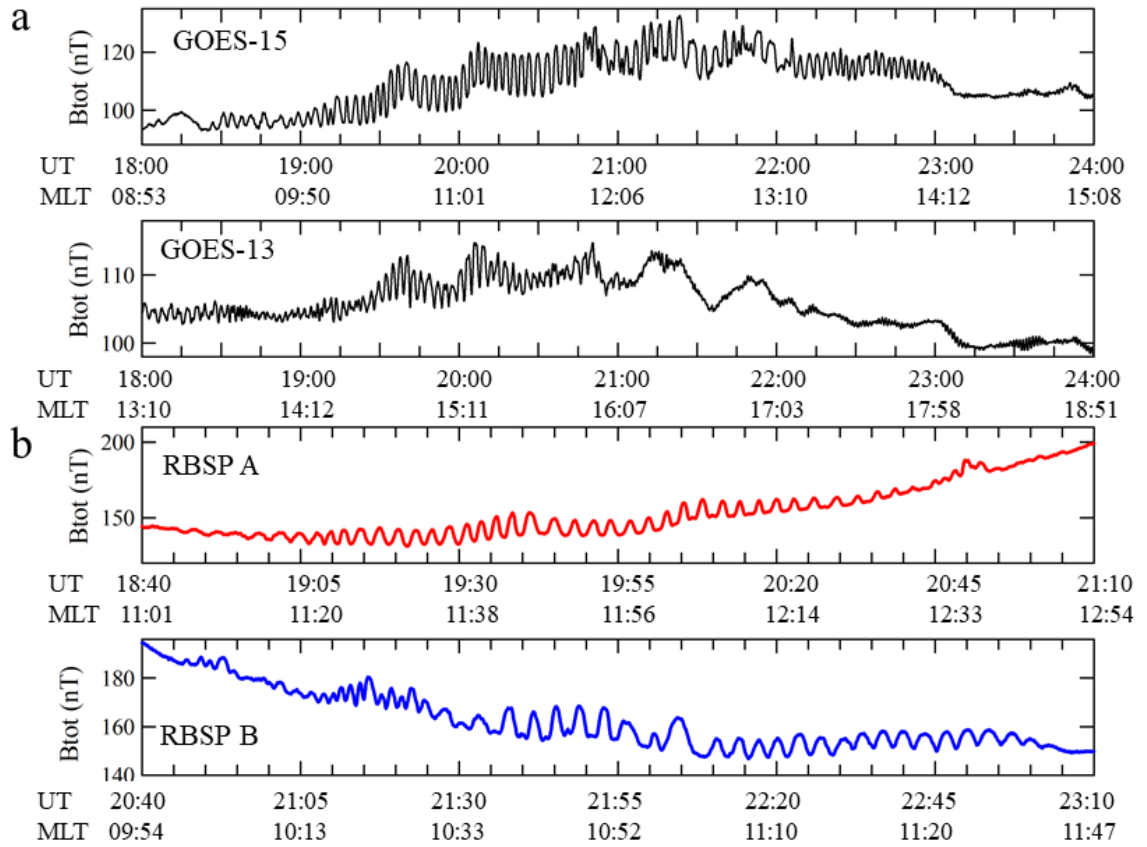


471
 472 Figure 2. Trajectories of RBSP-A (red) and -B (blue) and G-13 (black) and -15 (purple) from
 473 15:00 UT to 24:00 UT on January 1, 2016 in the X-Y and X-Z GSM planes. Open circles mark
 474 the beginning of the spacecraft trajectories which are duskward for the GOES spacecraft and
 475 duskward at apogee for the Van Allen Probes. The thick line segments indicate the locations of
 476 the spacecraft at the times when compressional Pc5 magnetic field pulsations occurred. Dots
 477 mark their locations where weak pulsations ($A < 5$ nT) occurred.
 478



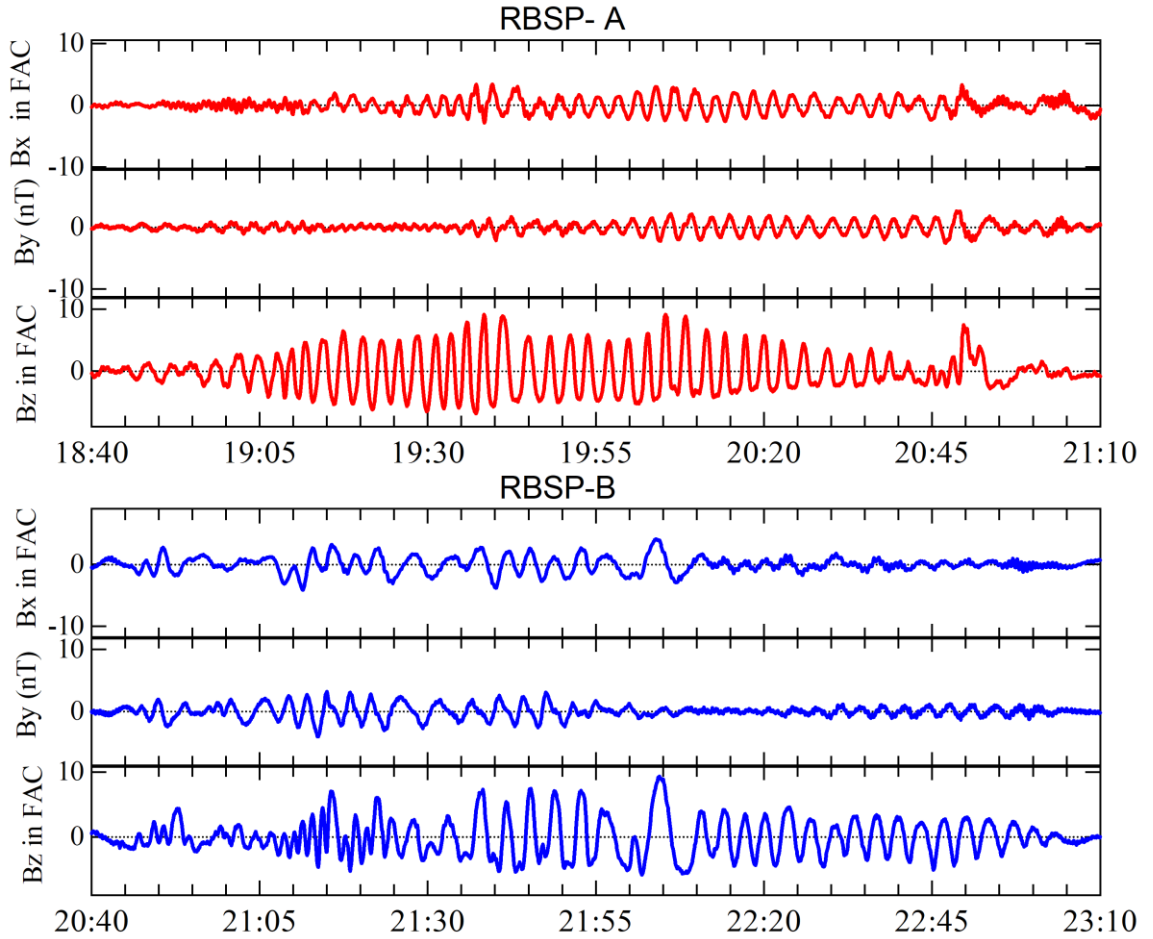
479

480 Figure 3. Observations of the solar wind dynamic pressure at Wind (time shifted) and the total
 481 magnetic field strength at G-13 and -15 from 18:00 UT to 24:00 UT. The arrows connect
 482 enhancements of the solar wind dynamic pressure to corresponding compressions of the
 483 magnetosphere.

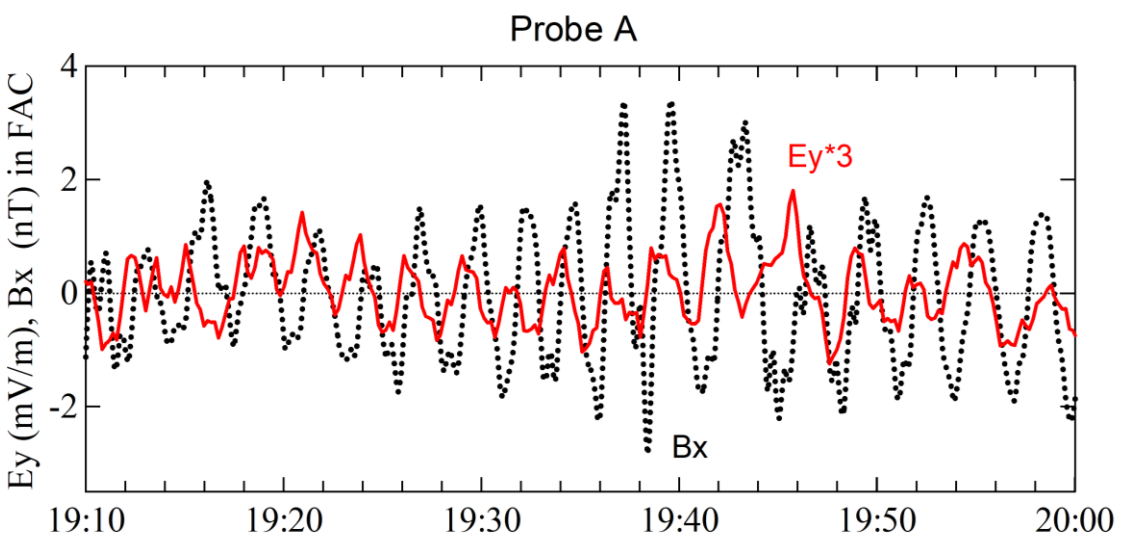


484

485 Figures 4 (a, b). G-15 and G-13 (a) total magnetic field strength from 18:00 UT to 24:00 UT on
 486 January 1, 2016. RBSP-A and -B (b) total magnetic field strength from 18:40 UT to 21:10 UT
 487 and from 20:40 UT to 23:10 UT on January 1, 2016, respectively. Beneath the panels are listed
 488 the universal time (UT) and magnetic local time (MLT).

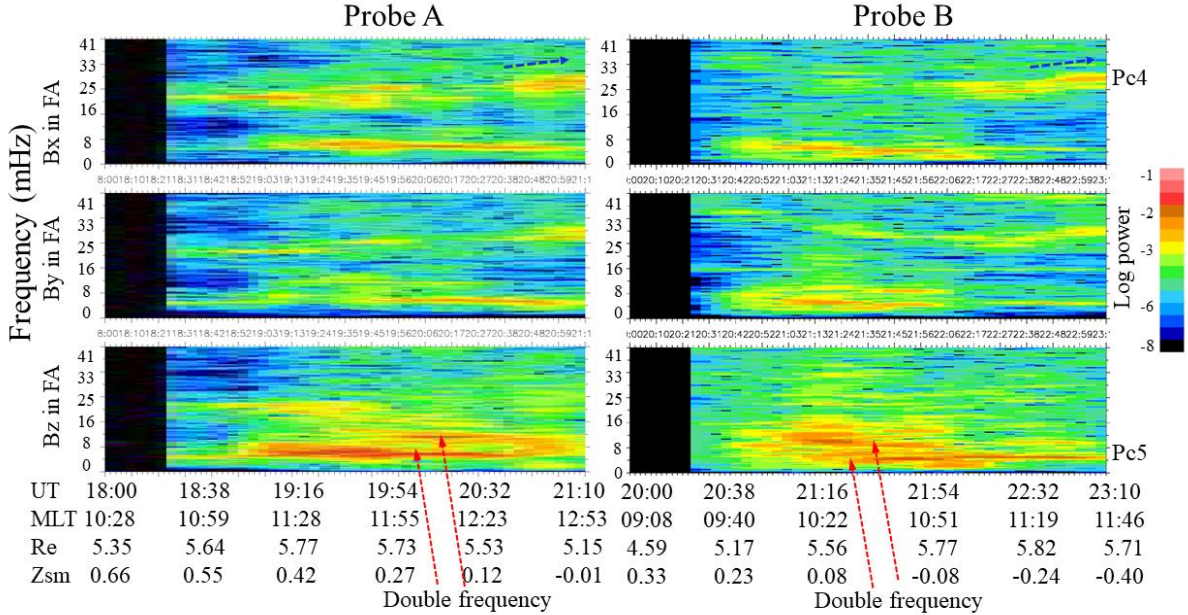


489
 490 Figure 5. RBSP-A and -B magnetic field observations in field-aligned coordinates from 18:40
 491 UT to 21:10 UT and from 20:40 UT to 23:10 UT on January 1, 2016, respectively.



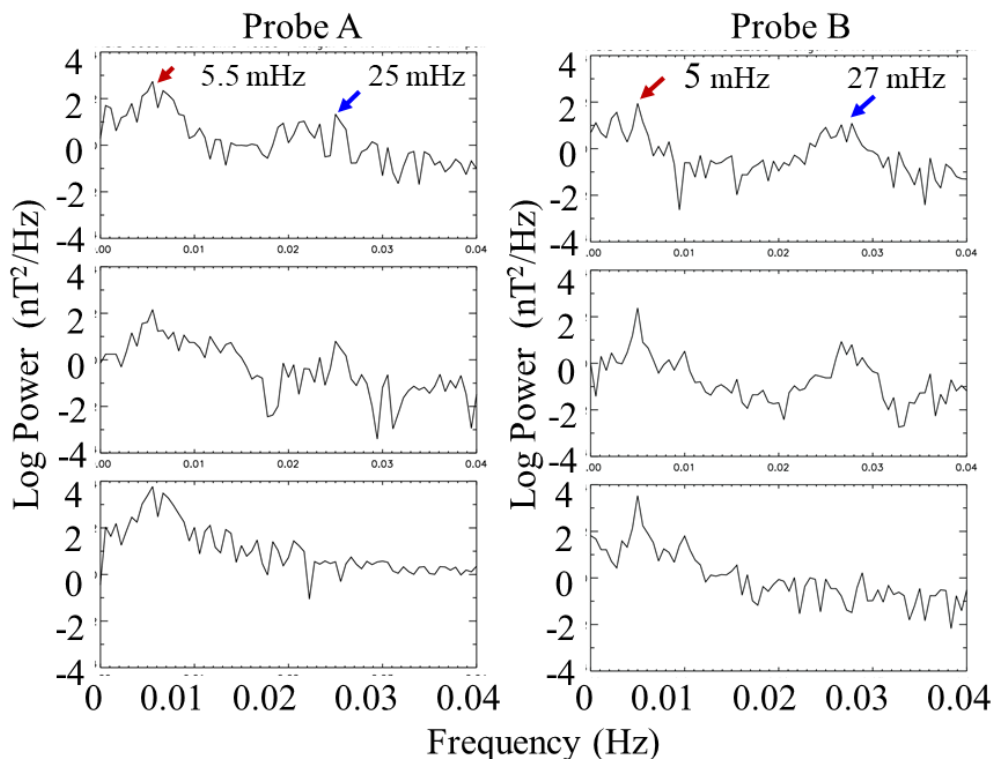
492

493 Figure 6. The phase difference between the RBSP-A azimuthal component of the electric field
 494 (red curve is boxcar smoothed) and the radial component of the magnetic field Bx in field-
 495 aligned coordinates (dashed curve) from 19:10 UT to 20:00 UT on January 1, 2016. The
 496 amplitude of Ey was multiplied by a factor of 3 to better display the visual effects.



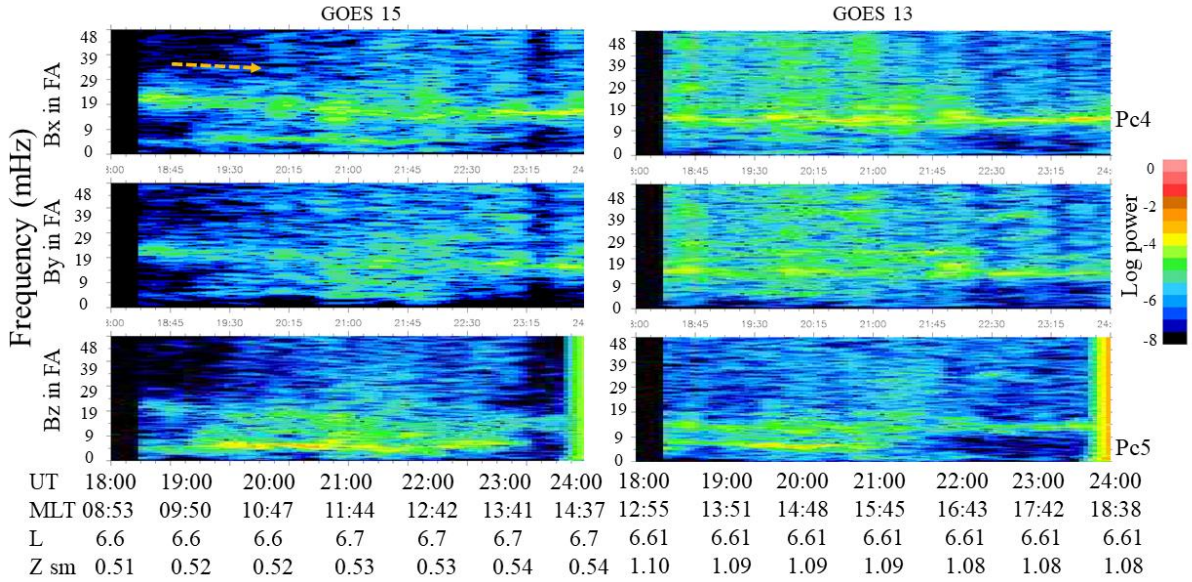
497

498 Figure 7. Three component dynamic spectra of magnetic field data at RBSP-A and -B from
 499 18:00 to 21:10 UT and from 20:00 UT to 23:10 UT on January 1, 2016, respectively. Beneath
 500 the panels are listed the universal time (UT), magnetic local time (MLT), radius (Re) and Z
 501 (SM) in Earth radius.

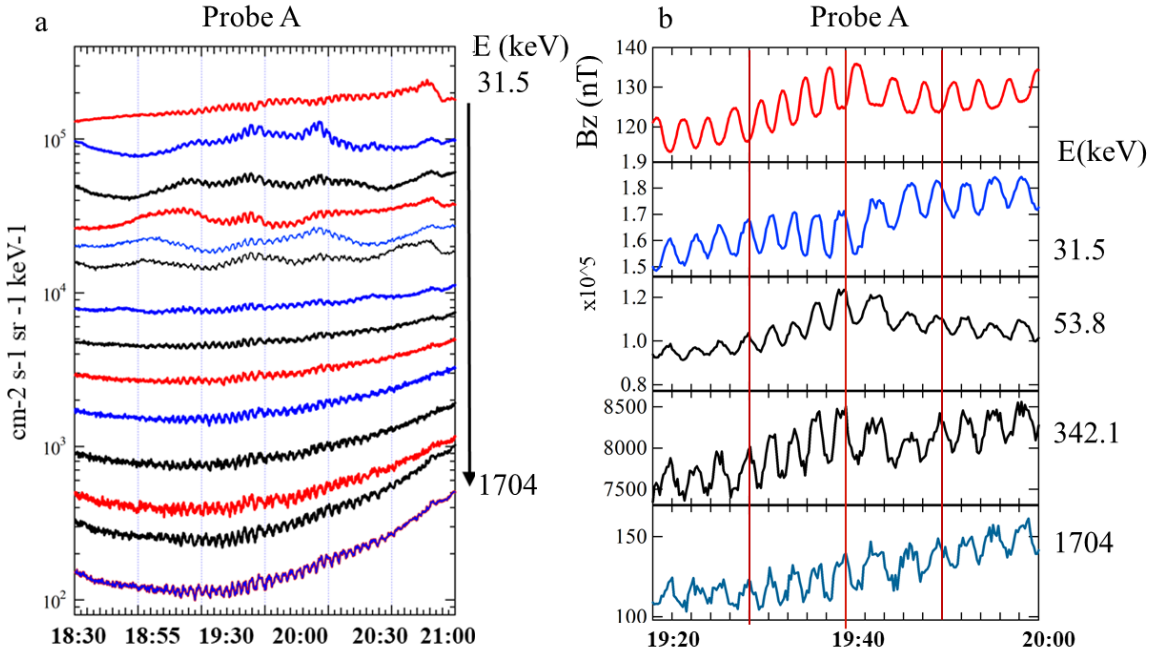


502

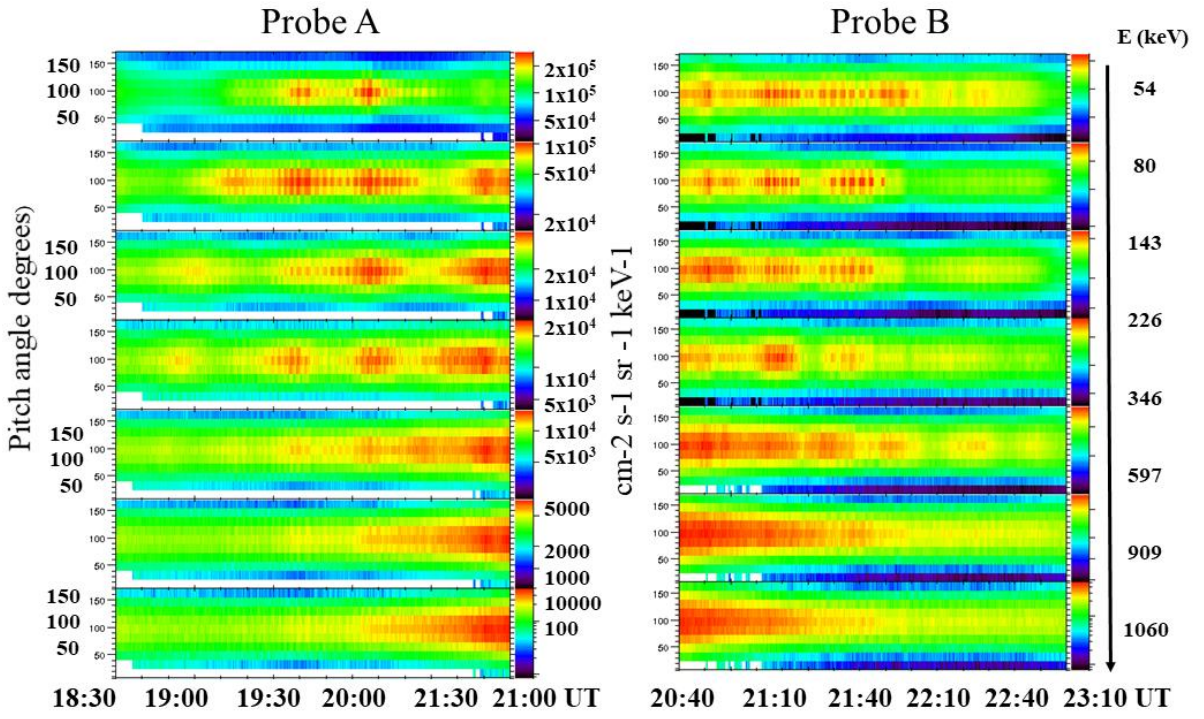
503 Figure 8. Fourier spectra calculated for the radial, azimuthal and compressional components of
 504 the RBSP-A and -B magnetic field in 5-minute sliding averaged mean field-aligned coordinates
 505 from 19:30 UT to 20:00 UT and from 22:30 UT to 23:00 UT on 1 January, 2016.



506
 507 Figure 9. Three components of dynamic spectra of the magnetic field data at G-15 and G-13
 508 from 18:00 UT to 24:00 UT on January 1, 2016. Beneath the panels are listed the universal
 509 time (UT), magnetic local time (MLT in SM), L and Z (SM) in Earth radii.

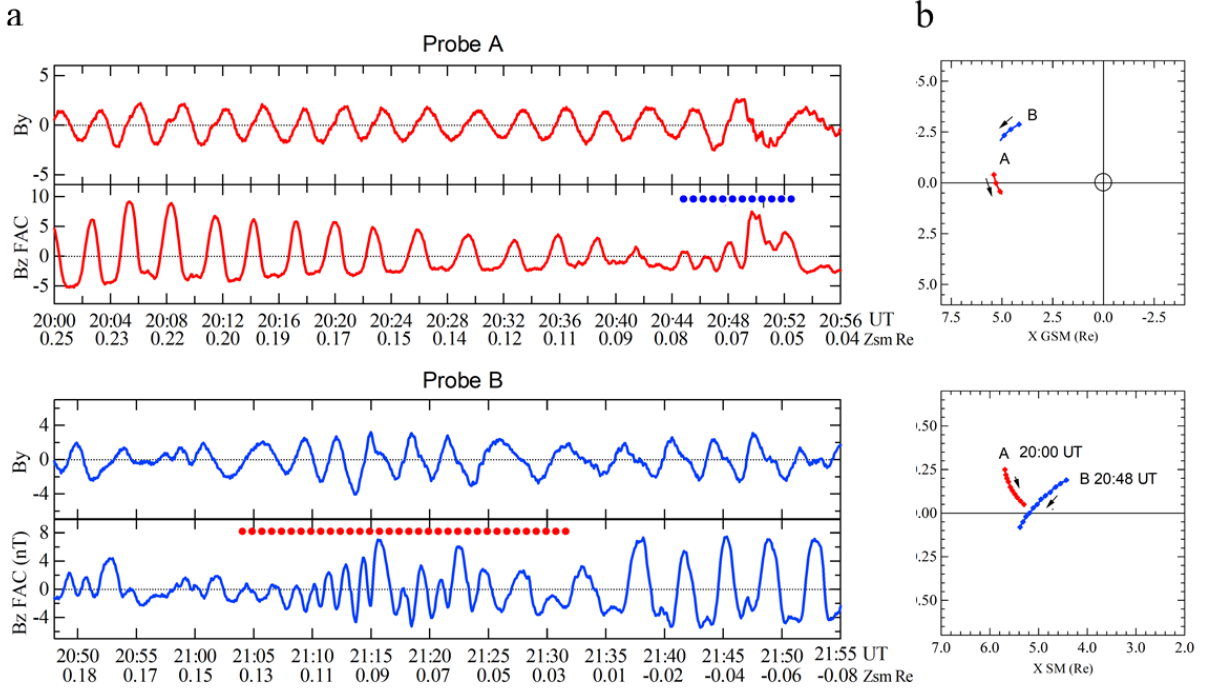


510
 511 Figures 10 (a, b). RBSP-A observations of electron fluxes (a) in the energy range from 31.5
 512 keV to 1704 keV from 18:30 UT to 21:00 UT and (b) their expanded view for selected energies
 513 from 19:20 UT to 20:00 UT.



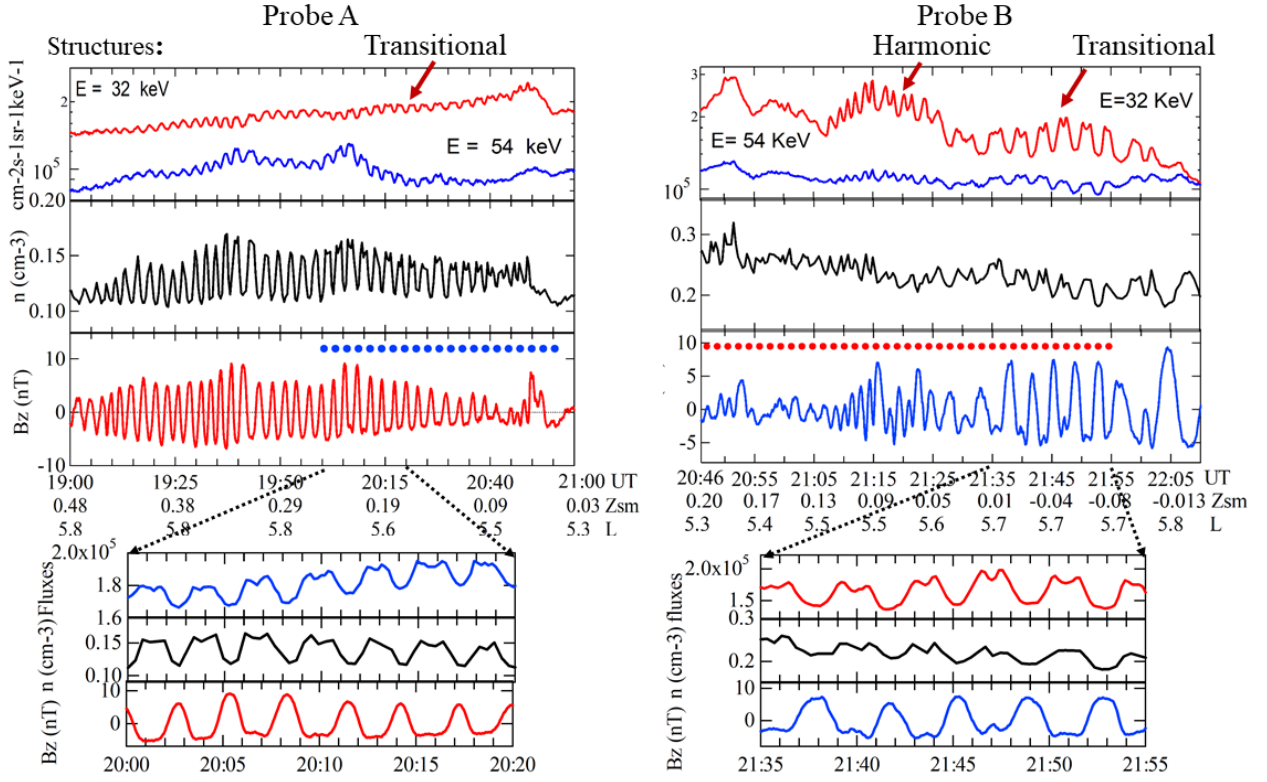
514

515 Figure 11. RBSP-A and -B observations of pitch-angle distributions for electrons in the energy
 516 range from 54 keV and 1060 keV from 18:30 to 21:00 UT and from 20:40 UT to 23:10 UT on
 517 January 1, 2016, respectively.



518

519 Figures 12 (a, b). RBSP-A and -B observations of double frequency pulsations (a) from 20:00 UT
 520 to 20:56 UT and from 20:48 UT to 21:55 UT, respectively, and (b) their locations in the X - Y
 521 GSM and X - Z SM planes. Red and blue dashed lines mark the intervals with harmonic
 522 structure of double-frequency pulsations.



524

525

526

527

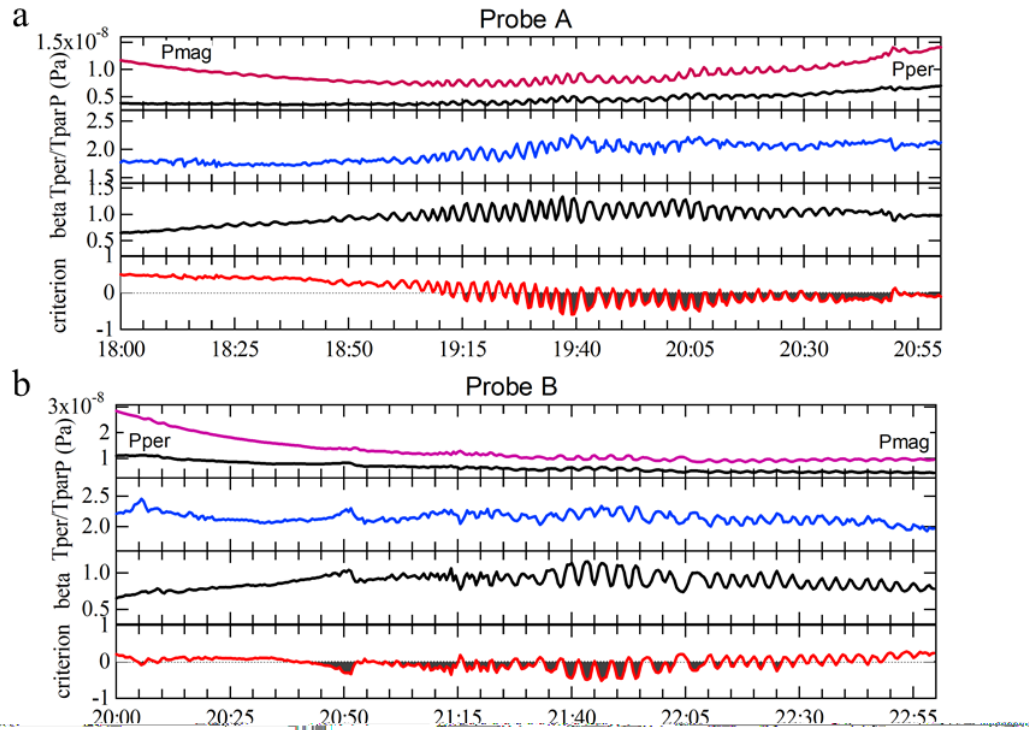
528

529

530

531

Figure 13. RBSP-A (left panel) and -B (right panel) presents electron fluxes for energies at 31.9 keV and 54.8 keV from EMFISIS, electron densities from HOPE and the Bz component of the magnetic field in field-aligned coordinates from MagEIS from 19:00 UT to 21:00 UT and from 20:46 UT to 22:10 UT, respectively. The panels in the bottom of the figure present expanded views of 20 min intervals with the double-frequency pulsations to better visualize their features.



532
533 Figures 14 (a, b). RBSP-A and -B plasma and magnetic field parameters characterizing the
534 pulsations. From top to bottom, the figure shows the magnetic pressure, perpendicular plasma
535 pressure, the ratio of the plasma temperatures perpendicular and parallel to the magnetic field,
536 beta, and the results for the mirror instability criterion on January 1, 2016. Shaded grey areas
537 indicate the times when the drift mirror instability is satisfied (< 1).

538
539 **Data availability.** Data used in the paper are available publicly at
540 http://cdaweb.gsfc.nasa.gov/istp_public/ (Coordinated Data Analysis Web, NASA, 2018). GOES
541 data were obtained from http://satdat.ngdc.noaa.gov/sem/goes/data/new_full/ (NOAA, 2018).
542 The electric field data were obtained from <http://www.space.umn.edu/rbspefw-data> (Wygant and
543 Breneman, 2017).

544
545 **Author contributions.** GK drafted and wrote the paper with participation of all coauthors. DS
546 conceived ideas, ME, ST, HS, CK –consulting regarding the data analysis, RR – software
547 development, MB–consulting regarding drift mirror instability test.

548 **Competing interests.** The authors have no conflict of interest.

549
550 **Acknowledgements.** The Van Allen Probes mission is supported by NASA. NASA GSFC's
551 CDAWEB provided Wind and GOES observations, while SSCWEB provided Van Allen Probes
552 EPHEMERIS. GK was supported by NASA contract no 80NSSC19K0440. M. A. B. is
553 grateful to the STFC (grant ST/R000697/1).

554
555 **References**

556 Blake, J. B., Carranza, P. A., Claudepierre, S. G., Clemons, J. H., Crain Jr., W. R., Dotan, Y.,
557 Fennell, J. F., Fuentes, F. H., Galvan, R. M., George, J. S., Henderson, M. G., Lalic, M.,
558 Lin, A. Y., Looper, M. D., Mabry, D. J., Mazur, J. E., McCarthy, B., Nguyen, C. Q.,

559 O'Brien, T. P., Perez, M. A., Redding, M. T., Roeder, J. L., Salvaggio, D. J., Sorensen, G.
560 A., Spence, H. E., Yi, S., and Zakrzewski, M. P.: The Magnetic Electron Ion Spectrometer
561 (MagEIS) Instruments Aboard the Radiation Belt Storm Probes (RBSP) Spacecraft, *Space*
562 *Sci. Rev.*, 179, 383–421, <https://doi.org/10.1007/s11214-013-9991-8>, 2013.

574 Chen, L., and Hasegawa, A.: Kinetic theory of geomagnetic pulsations.1. Internal excitations by
575 energetic particles, *J. Geophys. Res.*, 96, 1503–1512, <https://doi.org/10.1029/90JA02346>,
576 1991.

577 Cheng, C. Z. and Lin, C. S.: Eigenmode analysis of compressional waves in the magnetosphere,
578 *Geophys. Res. Lett.*, 8, 884–887, <https://doi.org/10.1029/GL014i008p00884>, 1987.

579 Cheng, C. Z., and Q. Qian, O.: Theory of ballooning-mirror mode instabilities for anisotropic
580 pressure plasmas in the magnetosphere, *J. Geophys. Res.*, 99, 11,193–11,210.,
581 <https://doi.org/10.1029/94JA00657>, 1994.

582 Coleman Jr., P. J.: Geomagnetic storms at ATS 1, in: Intercorrelated Satellite observations
583 related to solar events, edited by: Manno V., Page D.E. (eds), Intercorrelated Satellite
584 Observations Related to Solar Events. Astrophysics and Space Science Library, vol 19.
585 Springer, Dordrecht, https://doi.org/10.1007/978-94-010-3278-0_18, 1970.

586 Constantinescu, O. D., Glassmeier, K.-H., Plaschke, F., Auster, U., Angelopoulos, V.,
587 Baumjohann, W., Fornacon, K.-H., Georgescu, E., Larson, D., Magnes, W., McFadden,
588 J. P., Nakamura, R., Narita, Y.: THEMIS observations of dusk side compressional Pc 5
589 pulsations, *J. Geophys. Res.*, 114, A00C25, doi:10.1029/2008JA013519, 2009.

590 Cummings, W.D., O'Sullivan, R.J., and Coleman Jr., P.J.: Standing Alfvén waves in the
591 magnetosphere, *J. Geophys. Res.*, 74, 778 – 793, <https://doi.org/10.1029/JA074i003p00778>,
592 1969.

593 Dai, L., Takahashi, K., Wygant, J. R., Chen, L., Bonnell, J., Cattell, C. A., Thaller, S., Kletzing,
594 C., Smith, C. W., MacDowall, R.J., Baker, D.N., Blake, J. B., Fennell, J., Claudepierre, S.,
595 Funsten, H.O., Reeves, G.D., and Spence, H.E.: Excitation of poloidal standing Alfvén
596 waves through drift resonance wave-particle interaction, *Geophys. Res. Lett.*, 40, 4127–
597 4132, doi:10.1002/grl.50800, 2013.

598 Elkington, S. R., Hudson, M .K., and Chan, A. A.: Resonant acceleration and diffusion of outer
599 zone electrons in an asymmetric geomagnetic field, *J. Geophys. Res.*, 108(A3), 1116,
600 doi:10.1029/2001JA009202, 2003.

601 Engebretson, M., Glassmeier, K.– H., Stellmacher, M., Hughes, W. J., Lühr, H.: The
602 dependence of high-latitude PcS wave power on solar wind velocity and on the phase of
603 high-speed solar wind streams, *J. Geophys. Res.*, 103(A11), 26,271–26,283,
604 doi:10.1029/97JA03143, 1988.

605 Guo, X. C., Wang, C., and Hu, Y. Q.: Global MHD simulation of the Kelvin-Helmholtz
606 instability at the magnetopause for northward interplanetary magnetic field, *J. Geophys.*
607 *Res.*, 115, A10218, doi:10.1029/2009JA015193, 2010.

608 Hedgecock, P. C.: Giant Pc5 pulsations in the outer magnetosphere: A study of HEOS-1 data,
609 *Planet. Space Sci.*, 24, 921-935, [https://doi.org/10.1016/0032-0633\(76\)90003-9](https://doi.org/10.1016/0032-0633(76)90003-9), 1976.

610 Higbie, P.R., Baker, D.N., Zwickl, R.D., Bellian, R.D., Asbridge, J.R., Fennell, J.F., Wilken, B.,
611 and Arthur, C.W.: The Global Pc 5 Event of November 14–15, 1979, *J. Geophys. Res.*, 87,
612 2337–2345, <https://doi.org/10.1029/JA087iA04p02337>, 1982.

613 Higuchi, T., Kokubun, S., and Ohtani, S.: Harmonic structure of compressional Pc 5 pulsations
614 at synchronous orbit, *Geophys. Res. Lett.*, 13, 1101,
615 <https://doi.org/10.1029/GL013i011p01101>, 1986.

616 Kepko, L., and Spence, H. E.: Observations of discrete, global magnetospheric oscillations
617 directly driven by solar wind density variations, *J. Geophys. Res.*, 108, 1257,
618 doi:10.1029/2002JA009676, 2003.

619 Kivelson, M. G. and Southwood, D. J.: Charged particle behavior in low-frequency geomagnetic
620 pulsations, 4. Compressional waves, *J. Geophys. Res.*, 90, 1486–1498,
621 <https://doi.org/10.1029/JA090iA02p01486>, 1985.

622 Kletzing, C. A., Kurth, W. S., Acuna, M., MacDowall, R. J., Torbert, R. B., Averkamp, T.,
623 Bodet, D., Bounds, S. R., Chutter, M., Connerney, J., Crawford, D., Dolan, J. S., Dvorsky
624 R., Hospodarsky, G. B., Howard, J., Jordanova, V., Johnson, R. A., Kirchner, D. L.,
625 Mokrzycki, B., Needell, G., Odom, J., Mark, D., Pfaff Jr., Phillips, J. R., Piker, C. W.,
626 Remington, S. L., Rowland, D., Santolik, O., Schnurr, R., Sheppard, D., Smith, C. W.,
627 Thorne, R. M., and Tyler, J.: The Electric and Magnetic Field Instrument Suite and
628 Integrated Science (EMFISIS) on RBSP, *Space Sci. Rev.*, 179, 127–181,
629 doi:10.1007/s11214-013-9993-6, 2013.

630 Korotova, G. I., Sibeck, D. G., Angelopoulos, V., and Walsh, W.: Themis observations of
631 compressional poloidal pulsations in the dawnside magnetosphere: a case study, *J. Geophys.*
632 *Res.*, 118, 7665–7673, doi:10.1002/2013JA019360, 2013.

633 Kokubun, S., Statistical characteristics of Pc 5 waves at geostationary orbit, *J. Geomag.*
634 *Geoelectr.*, 37, 759–779, <https://doi.org/10.5636/jgg.37.759>, 1985.

635 Kremser, G., Korth, A., Feier, J. A., Wilken, B., Gurevich, A. V., and Amata, E.: Observations
636 of quasi-periodic flux variations of energetic ions and electron associated with Pc5
637 geomagnetic pulsations, *J. Geophys. Res.*, 86, 3345–3356,
638 <https://doi.org/10.1029/JA086iA05p03345>, 1981.

639 Lanzerotti, L. J., Hasegawa, A., and MacLennan, C. G.: Drift mirror instability in the
640 magnetosphere: Particle and field oscillations and electron heating, *J. Geophys. Res.*, 74,
641 5565–5578, <https://doi.org/10.1029/JA074i024p05565>, 1969.

642 Lin, C. S., Parks, G. K., and Winckler J. R.: The 2-to12-min quasi-periodic variation of 50-to
643 1000-keV trapped electron fluxes, *J. Geophys. Res.*, 81(25), 4517–4523,
644 <https://doi.org/10.1029/JA081i025p04517>, 1976.

645 Lin, C. S. and Parks, G. K.: The coupling of Alfvén and compressional waves, *J. Geophys. Res.*,
646 83, 2628–2636, <https://doi.org/10.1029/JA083iA06p02628>, 1978.

647 Liu, H., Zong, Q.-G., Zhou, X. Z., Fu, S. Y., Rankin, R., Wang, L.-H., Yuan C. J., Wang, Y. F.,
648 Baker, D. N., Blake, J. B., and Kletzing, C. A. : Compressional ULF wave modulation of
649 energetic particles in the inner magnetosphere. *Journal of Geophysical Research: Space*
650 *Physics*, 121, 6262–6276, <https://doi.org/10.1002/2016JA022706>, 2016.

651 Lin, R. P., Anderson, K. A., Ashford S., Carlson, C., Curtis, D., Ergun, R., Larson, D.,
652 McFadden, J., McCarthy, M., Parks, G. K., Rème, H., Bosqued, J. M., Coutelier, J.,
653 Cotin, F., Wenzel, K.-P., Sanderson, T. R., Henrion, J., Ronnet, J. C., Paschmann, G.: A
654 three-dimensional (3-D) plasma and energetic particle experiment for the Wind spacecraft of
655 the ISTP/GGS mission, *Space Sci. Rev.*, 71, 125–153, <https://doi.org/10.1007/BF00751328>,
656 1995.

657 Lepping, R.P., Acuna, M.H., Burlaga, L.F., Farrell, W.M., Slavin, J. A., Schatfen, K. H.,
658 Mariani, E., Ness, N. E., Neubauer, E. M., Whang, Y. C., Byrnes J. B., Kennon R. S.,
659 Panetta, P. V., Scheifele J., and Worley, E. M.: The WIND Magnetic field investigation,
660 *Space Sci. Rev.*, 71, 207–229, <https://doi.org/10.1007/BF00751330>, 1995.

661 Mauk, B. H., Fox, N. J., Kanekal, S. G., Kessel, R. L., Sibeck, D. G., and Ukhorskiy, A.: Science
662 objectives and rationale for the radiation belt storm probes mission, *Space Sci. Rev.*, 179, 3–
663 27, doi:10.1007/s11214-012-9908-y, 2012.

664 Mitchell, D.G., Lanzerotti, L.J., Kim, C.K., Stokes, M., Ho, G., Cooper, S., Ukhorskiy, A.,
665 Manweiler, J.W., Jaskulek, J., Haggerty, D.K., Brandt, P., Sitnov, M., Keika, K., Hayes,
666 J.R., Brown, L.E., Gurnee, R.S., Hutcheson, J.C., Nelson, K.S., Paschalidis, N., Rossano,
667 E., Kerem, S.: Radiation belt storm probes ion composition experiment (RBSPICE), *Space*
668 *Sci. Rev.*, 179, 263–308, doi:10.1007/s11214-013-9965-x, 2013.

669 Motoba, T., Kikuchi, T., Okuzawa, T., and Yumoto, K.: Dynamical response of the
670 magnetosphere-ionosphere system to a solar wind dynamic pressure oscillation, *J. Geophys.*
671 *Res.*, 108(A5), 1206, doi:10.1029/2002JA009696, 2003.

672 Nagano, H. and Araki, T.: Long-duration Pc5 pulsations observed by geostationary satellites,
673 *Geophys. Res. Lett.*, 10, 908–911, <https://doi.org/10.1029/GL010i009p00908>, 1983.

674 NASA: Coordinated Data Analysis Web, available at: http://cdaweb.gsfc.nasa.gov/istp_public/,
675 last access: 1 March 2020.

676 NOAA: GOES SEM fata, available at: http://satdat.ngdc.noaa.gov/sem/goes/data/new_full/, last
677 access: 2 January 2019.

678 Pokhotelov, O. A., Pilipenko, V. A., Nezlina, I. M., Woch, J., and Kremser, G.: Excitation of
679 high β plasma instabilities at the geostationary orbit: Theory and observations, *Planet. Space
680 Sci.*, 34, 695–712, [https://doi.org/10.1016/0032-0633\(86\)90124-8](https://doi.org/10.1016/0032-0633(86)90124-8), 1986.

681 Samson, J. C., Harrold, B. G., Ruohoniemi, J. M., Greenwald, R. A., and Walker, A. D. M.:
682 Field line resonance associated with MHD waveguides in the magnetosphere, *Geophys. Res.
683 Lett.*, 19, 441–444, <https://doi.org/10.1029/92GL00116>, 1992.

684 Sarris, T.E., Liu, W., Li, X., Kabin, K., Talaat, E.R., Rankin, R., Angelopoulos, V.,
685 Bonnell, J., Glassmeier, K.-H.: THEMIS observations of the spatial extent and
686 pressure-pulse excitation of field line resonances, *Geophys. Res. Lett.*, 37, L15104,
687 <https://doi.org/10.1029/2010GL044125>, 2010.

688 Singer, H.J., Matheson, L., Grubb, R., Newman, A., and Bouwer, S. D.: Monitoring space
689 weather with the GOES magnetometers, in: SPIE Conference Proceedings, vol. 2812, edited
690 by: Washwell, E. R., 299–308, GOES-8 and Beyond SPIE, Bellingham, WA, USA, 1996.

691 Shen, X.-C., Shi, Q., Wang, B., Zhang, H., Hudson, M. K., Nishimura, Y., Hartinger, M. D.,
692 Tian, A., Zong, Q.G., Rae, I. J., and Degeling, A. W.: Dayside magnetospheric and
693 ionospheric responses to a foreshock transient on 25 June 2008: 1. FLR observed by satellite
694 and ground-based magnetometers. *Journal of Geophysical Research: Space Physics*, 123,
695 6335–6346. <https://doi.org/10.1029/2018JA025349>, 2018.

696 Southwood, D. J., Dungey, J. W., and Etherington, R. J.: Bounce resonance interaction between
697 pulsations and trapped particles, *Planet. Space Sci.*, 17, 349–361,
698 [https://doi.org/10.1016/0032-0633\(69\)90068-3](https://doi.org/10.1016/0032-0633(69)90068-3), 1969.

699 Southwood, D. J.: The behaviour of ULF waves and particles in the magnetosphere, *Planet.
700 Space Sci.*, 21, 53–65, [https://doi.org/10.1016/0032-0633\(73\)90019-6](https://doi.org/10.1016/0032-0633(73)90019-6), 1973.

701 Southwood D.J.: Low Frequency Pulsation Generation by Energetic Particles, *Advances in
702 Earth and Planetary Sciences*, vol 11. Springer, Dordrecht,
703 https://doi.org/10.1007/978-94-009-8426-4_5, 1981.

704 Southwood, D. J. and Kivelson, M. G.: Mirror instability: 1. Physical mechanism of linear
705 instability, *J. Geophys. Res.*, 98, 9181–9187, <https://doi.org/10.1029/92JA02837>, 1993.

706 Spence, H. E., Reeves, G. D., Baker, D. N., Blake J. B., Bolton, M., Bourdarie, S., Chan, S. G.,
707 Claudpierre, S. G., Clemons, J. H., Cravens, J. P., Elkington, S. R., Fennell, J. F., Friedel,
708 R. H. W., Funsten, H. O., Goldstein, J., Green, J. C., Guthrie, A., Henderson, M. G., Horne,

709 R. B., Hudson, M. K., Jahn, J.-M., Jordanova, V. K., Kanekal, S. G., Klatt, B. W., Larsen, B.
710 A., Li, X., MacDonald, E. A., Mann, I. R., Niehof, J., O'Brien, T. P., Onsager, T. G.,
711 Salvaggio, D., Skoug, R. M., Smith, S. S., Suther, L. L., Thomsen, M. F., and Thorne R. M.:
712 Science goals and overview of the Energetic Particle, Composition, and Thermal Plasma
713 (ECT) Suite on NASA's Radiation Belt Storm Probes (RBSP) Mission, *Space Sci. Rev.*,
714 179, 311–336, doi:10.1007/s11214013-0007-5, 2013.

715 Sugiura, M., and Wilson, C. R.: Oscillation of the geomagnetic field lines and associated
716 magnetic perturbations at conjugate points, *J. Geophys. Res.*, 69, 1211–1216,
717 <https://doi.org/10.1029/JZ069i007p01211>, 1964.

718 Takahashi, K., McPherron, R. L., Hughes, W. J.: Multispacecraft observations of the harmonic
719 structure of Pc 3–4 magnetic pulsations, *J. Geophys. Res.*, 89, 6758–6774,
720 <https://doi.org/10.1029/JA089iA08p06758>, 1984.

721 Takahashi, K., Higbie, P. R., and Baker, D. N.: Azimuthal propagation and frequency
722 characteristic of compressional Pc 5 waves observed at geostationary orbit, *J. Geophys.
723 Res.*, 90, 1473–1485, <https://doi.org/10.1029/JA090iA02p01473>, 1985.

724 Takahashi, K., and Higbie, P. R.: Antisymmetric standing wave structure associated with the
725 compressional Pc 5 pulsation of November 14, 1979, *J. Geophys. Res.*, 91, 11163–11178,
726 <https://doi.org/10.1029/JA091iA10p11163>, 1986.

727 Takahashi, K., Fennell, J. F., Amata, E., Higbie, P. R.: Field-aligned structure of the storm time
728 Pc5 wave of November 14–15, 1979, *J. Geophys. Res.*, 92, 5857–5864,
729 <https://doi.org/10.1029/JA092iA06p05857>, 1987a.

730 Takahashi, K., L. J. Zanetti, T. A. Potemra, and M. H. Acuña: A model for the harmonic of
731 compressional Pc5 waves, *Geophys. Res. Lett.*, 14, 363–366,
732 <https://doi.org/10.1029/GL014i004p00363>, 1987b.

733 Takahashi, K., Cheng, C. Z., McEntire, R. W., and Kistler, L. M.: Observation and theory of Pc5
734 waves with harmonically related transverse and compressional components, *J. Geophys.
735 Res.*, 95, 977–989, <https://doi.org/10.1029/JA095iA02p00977>, 1990.

736 Takahashi, K., Glassmeier, K.-H., Angelopoulos, V., Bonnell, J., Nishimura, Y., Singer, H.
737 J., and Russell, C. T.: Multisatellite observations of a giant pulsation event, *J. Geophys.
738 Res.*, 116, A11223, doi:10.1029/2011JA016955, 2011.

744 Vaivads, A., Baumjohann, W., Haerendel, G., Nakamura, R., Kucharek, H., Klecker, B.,
745 Lessard, M.R., Kistler, L. M., Mukai, T., and A. Nishida, A: Compressional Pc5 type
746 pulsations in the morning plasma sheet, *Ann. Geophys.*, 19, 311–320,
747 <https://doi.org/10.1029/2001JA900042>, 2001.

748 Walker, A. D. M., Greenwald, R. A., Korth, A., Kremser, G.: STARE and GEOS 2 observations
749 of a storm time Pc5 ULF pulsation, *J. Geophys. Res.*, 87, 9135–9146,
750 <https://doi.org/10.1029/JA087iA11p09135>, 1982.

751 Wang, B., Nishimura, Y., Hietala, H., Shen, X.-C., Shi, Q., Zhang, H., Lyons, L., Zou, Y.,
752 Angelopoulos, V., Ebihara, Y., Weatherwax, A.: Dayside magnetospheric and ionospheric
753 responses to a foreshock transient on 25 June 2008: 2. 2-D evolution based on dayside
754 auroral imaging. *Journal of Geophysical Research: Space Physics*, 123, 6347–6359.
755 <https://doi.org/10.1029/2017JA024846>, 2018.

756 Zhang, X. Y., Zong, Q.-G., Wang, Y. F., Zhang, H., Xie, L., Fu, S. Y., Yuan, C. J., Yue, C.,
757 Yang, B., and Pu, Z. Y.: ULF waves excited by negative/positive solar wind dynamic
758 pressure impulses at geosynchronous orbit, *J. Geophys. Res.*, 115, A10221,
759 <https://doi.org/10.1029/2009JA015016>, 2010.

760 Zhu, X. M. and Kivelson, M. G.: Compressional ULF waves in the outer magnetosphere: 1.
761 Statistical study. *J. Geophys. Res.*, 96, 19451–19467, <https://doi.org/10.1029/91JA01860>,
762 1991.

763

764